Time Delay of Wide Area Damping Control in Urban Power Grid: Model-Based Analysis and Data-Driven Compensation

Buxin She, Yuqing Dong* and Yilu Liu

Department of Electrical Engineering and Computer Science, The University of Tennessee, Knoxville, TN, United States
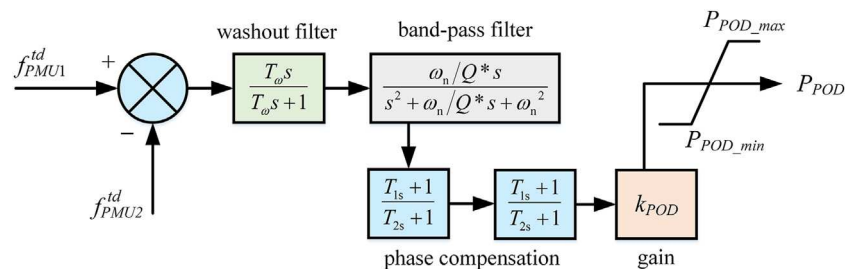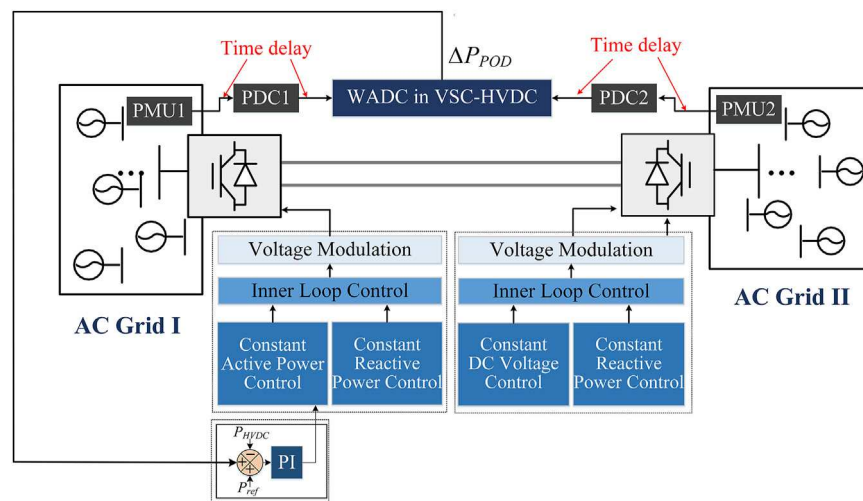
Due to the rapid development of economies, large urban cities consume an increasing amount of energy and have a higher requirement for power quality. Voltage source converter based high voltage direct current (VSC-HVDC) is a promising device to transmit clean power from remote regions to urban power systems, while also providing wide area damping control (WADC) for frequency stabilization. However, the time-delay naturally existing in the VSC-HVDC system may degrade the performance of WADC and even result in instability. To address this issue, this paper develops a time-delay correction control strategy for VSC-HVDC damping control in urban power grids. First, a small signal model of WADC is built to analyze the negative impacts of time delay. Then, a data-driven approach is proposed to compensate for the inherent time delay in VSC-HVDC damping control. The extensive training data will be generated under various disturbances. After offline training, the long short-term memory network (LSTM) can be implemented online to predict the actual frequency deviation based on real-time measurements. Finally, the proposed method is validated through MATLAB-Simulink in a two-area four-machine system. The results indicate that the data-driven compensation has a strong generalization ability for random delay time constants and can improve the performance of WADC significantly.

Keywords: wide area damping control, HVDC, small signal modeling, time delay compensation, long short-term memory
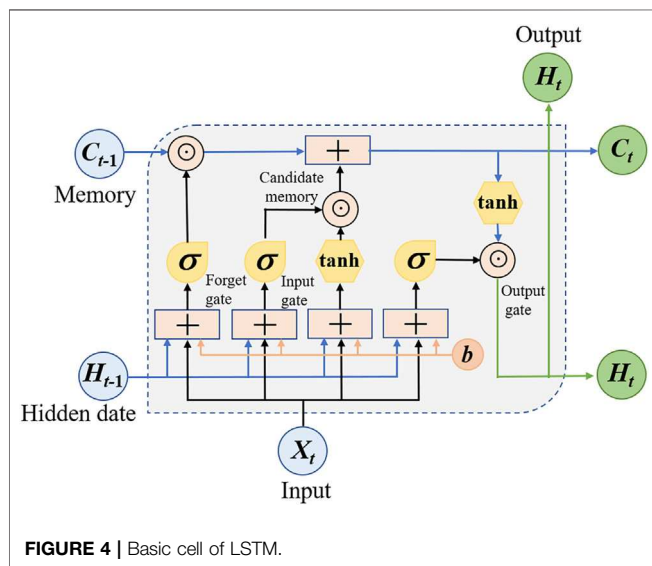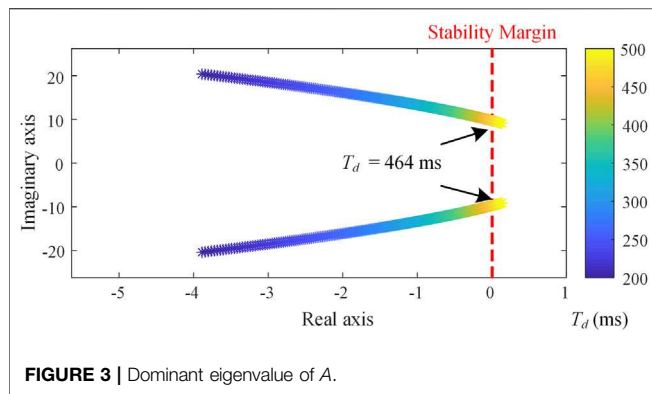
INTRODUCTION

Urbanization has witnessed the development of modern civilization (Jiang et al., 2019). Urban power grids are accommodating more people and consuming more energy than ever before (Xiao et al., 2022). With distributed energies and loads from distant areas (Pan et al., 2021; Sun et al., 2022; Yang et al., 2022), VSC-HVDC has been widely used to transmit clean energy from remote regions to urban power (Fu et al., 2021; Sun et al., 2021b; Xiao et al., 2021). On the other hand, the increasing uncertainty of distributed energy resources (Li S. et al., 2021; Zhang J. et al., 2022), extreme weather, and flexible loads like electrical vehicles pose great challenges to the frequency regulation of urban power grids (Xiong et al., 2021). With the interconnection of different regions of power grids, the inter-area low-frequency oscillations have also become a serious issue that threatens the system's stability (Baltas et al., 2021).

Wide area damping control (WADC) provides a promising approach to mitigate the oscillations of frequency and thus improve the stability of urban power grids (Li and Chen, 2018). However, in

FIGURE 1 | System diagram of VSC-HVDC.

FIGURE 2 | Control diagram of WADC.

WADC, the control signals measured by phasor measurement unit (PMU) are transmitted from a distant region through communication channels, which may bring an unavoidable time delay (Musleh et al., 2018). Such kind of delay can vary from tens to hundreds of milliseconds (He et al., 2009), depending on different communication distances, protocols, and measuring devices. Some research have reported that the existing time delay, even with a small value, will result in the loss of WADC control and power system instability (Xu et al., 2020). Considering the fast power controllability of VSC-HVDC (Sun et al., 2021a; Dong et al., 2021), the time delay in the control signal may bring a more destabilizing influence than other devices.

Some control strategies have been proposed to deal with the time delay in WADC. One of the conventional methods focuses on the offline parameter optimization of WADC, based on linear matrix inequality theory (LMI) (Chang et al., 2006; Li et al., 2010), Smith Predictor (Chaudhuri et al., 2004) and robust control strategies (Wang et al., 2010), which usually relies on known models and uses fixed parameters. To adapt to the varying conditions of the system operation, some adaptive control strategies are put forward to compensate the time delay more realistically (Cheng et al., 2014) (Zhu et al., 2016). The main idea of the adaptive control is to schedule the control gains and the phase compensation parameters

according to the online identification of the system model and oscillation modes. Nevertheless, the model estimation requires characteristic extraction from continuous ambient data injection, which may be influenced by system background noise and is not necessarily accurate and instantaneous.

Recently, the rapid development of artificial intelligence has created the potential for time delay compensation with neural networks. Among the various neural networks, the long short-term memory network (LSTM) is a kind of modern recurrent neural network that is designed for handling time series data (Xu et al., 2021). It has been successfully employed in power systems for islanding detection (Abdelsalam et al., 2020), load and generation forecast (Liu et al., 2020)-(Alavi et al., 2021), fast event identification (Li Z. et al., 2021), and measurements prediction (Wang et al., 2021). One common feature of these studies is that they made the best use of the time-series properties of power system data. Actually, the delayed PMU measurements are awesome time series data that can help predict the real time frequency deviation for WADC. Apart from LSTM, multilayer perception (MLP) and convolutional network (CNN) may also be used to predict delayed signals. However, MLP suffers from the computational burden when dealing with time-series data, and CNN cannot preserve the long-term information and skip the

FIGURE 3 | Dominant eigenvalue of A.

FIGURE 4 | Basic cell of LSTM.

builds up the small signal model of WADC with time delay and analyzes the negative impacts based on eigenvalue analysis. In *Data-Driven Delay Compensation With LSTM Section*, a data-driven delay compensation approach is developed using LSTM. *Case Study Section* validates the proposed method in a two-area four machine system with a comprehensive test. Finally, conclusions are drawn in *Conclusion Section*.

MODEL-BASED ANALYSIS ON TIME DELAY OF WIDE AREA DAMPING CONTROL

Wide Area Damping Control With Time Delay

With the large-scale application of PMU measurement and power electronics technology, VSC-HVDC has been widely used in the field of WADC. The typical framework is shown in **Figure 1**. According to the frequency data collected by the PMUs in different regions, the WADC adjusts the DC power reference value to suppress the inter-area low-frequency oscillations.

In **Figure 1**, f_{PMU1}, f_{PMU2} are the real-time frequencies collected by PMU1 and PMU2, respectively. f_{PMU1}^{td} and f_{PMU2}^{td} are the delayed frequencies after passing through the communication channels. The workflow of WADC in VSC-HVDC consists of the following five steps:

- The PMU configured in the AC grid measures the three-phase bus voltage and calculates the bus frequency.
- After data packaging, the frequency data from different PMUs is transmitted to the phase data concentrators (PDCs). During the transmission process, a special communication protocol, such as IEEE C37.118, is used to ensure the transmission security and accuracy.
- The PDC then unpacks the frequency data and sends it to the WADC of the VSC-HVDC.
- **Figure 2** illustrates the block diagram of the WADC. It consists of a washout block, a band-pass filter, two phase compensation blocks, and a gain block. The input of the controller is the difference between the frequencies collected by the two PMUs; while the output of the controller is the active power reference value P_{POD}. The time constant T_ω of the washout filter is chosen as 10s. In the band-pass filter, ω_n is the system oscillation frequency, and Q is the quality factor, which is usually set as 1. For active power modulation, the time constant in the compensation block can be considered as the same value, i.e., $T_{1s} = T_{2s}$; k_{POD} is the controller gain. P_{POD_max} and P_{POD_min} are the output limits of the WADC.
- P_{POD} will then be added as an auxiliary signal to the P_{ref} of the VSC-HVDC outer loop control to modulate the DC active power.

In the practical system operation, the time delay exists from PMU to PDC, and then to the WADC.

short-term input at the same time. Hence, this paper tries to integrate LSTM into the time delay compensation of urban VSC-HVDC systems. Compared with the existing literature, this paper has the following contributions.

- Formulated a small signal model of WADC with time delay and mathematically proved that the uncorrected PUM signals can result in the instability of the urban power grids.
- Proposed a data-driven delay compensation approach for WADC, leveraging the modern recurrent neural network LSTM. A well-trained LSTM was implemented online for time delay compensation after thorough offline training under various disturbances.
- Verified the proposed method through numerical simulation. Results showed that the LSTM-based compensation method has strong generalization ability. It can adapt to random delay time in real system even though the delay time constants were not included in the training dataset.

The rest of this paper is organized as follows. *Model-Based Analysis on Time Delay of Wide Area Damping Control Section*

Small Signal Modeling

In order to quantitatively analyze the influence of the time delay in VSC-HVDC system, a small signal model of VSC-HVDC with WADC considering the time delay has been established. In the test system, two generators are modeled to represent the two distant areas. A VSC station is connected to the two areas through transmission lines. The control strategy of the VSC-HVDC includes the WADC, outer loop control, inner loop control, and phase-locked loop (PLL).

For the generators in two areas, the rotor motion equations are shown in (**Eq. 1**).

$$\begin{cases} \dfrac{d\delta_{1,2}}{dt} = \omega_{g1,2} - \omega_0 \\[2mm] T_{J1,2}\dfrac{d\omega_{g1,2}}{dt} = T_{m1,2} - T_{e1,2} - D_{1,2}\omega_{g1,2} \end{cases} \tag{1}$$

where $\delta_{1,2}$ and $\omega_{g1,2}$ are the rotor phase and rotor angular velocity of the two generators. $T_{J1,2}$ is the inertia time constant; $D_{1,2}$ is the damping coefficient; $T_{m1,2}$ is the mechanical torque; while $T_{e1,2}$ is the electrical torque.

In the test system, the PMUs collect the frequencies at the ports of the two generators, so it can be considered that f_{PMU1}, f_{PMU2} are consistent with the corresponding generator frequencies, as shown in (**Eq. 2**).

$$\omega_{g1,2} = 2\pi f_{PMU1,2} \tag{2}$$

After the time delay, the difference between f_{PMU1}^{td} and f_{PMU2}^{td} is taken as the input to the WADC. The total time delay of the frequency difference can be assumed as T_d. Since the transfer function e^{-sT_d} is nonlinear, a fourth-order Pade approximation can be utilized to represent the characteristics of the time delay (Xu et al., 2020).

$$\frac{f_{error}^{td}}{f_{error}} = e^{-sT_d} \approx \frac{(T_ds)^4 - 20(T_ds)^3 + 180(T_ds)^2 - 840(T_ds) + 1680}{(T_ds)^4 + 20(T_ds)^3 + 180(T_ds)^2 + 840(T_ds) + 1680} \tag{3}$$

where $f_{error} = f_{PMU1} - f_{PMU2}$.

The state space equation of the Pade approximation can be transformed from (**Eq. 3**).

$$\begin{cases} \dfrac{d}{dt}z_p = A_p z_p + B_p u_p \\[2mm] y_p = C_p z_p + D_p u_p \end{cases} \tag{4}$$

Eq. 4 introduces four state variables $z_p = [z_1\ z_2\ z_3\ z_4]^T$; the input variable $u_p = f_{error}$; the output variable is $y_p = f_{error}^{td}$.

The delayed frequency signal can then be expressed as (5):

$$\begin{aligned} f_{error}^{td} &= -\frac{40}{T_d}z_1 - \frac{1680}{T_d^3}z_3 + f_{error} \\ &= -\frac{40}{T_d}z_1 - \frac{1680}{T_d^3}z_3 + \frac{1}{2\pi}(\omega_{g1} - \omega_{g2}) \end{aligned} \tag{5}$$

where f_{error}^{td} is the actual input of the WADC. The output P_{POD} will be superimposed on the active power reference value of VSC outer loop control. The transfer function of WADC can be described in (**Eq. 6**):

$$P_{POD} = k_{POD} \cdot \frac{T_\omega s}{T_\omega s + 1} \frac{\omega_n/Q \cdot s}{s^2 + \omega_n/Q \cdot s + \omega_n^2} f_{error}^{td} \tag{6}$$

Transforming it into the state space form:

$$\frac{d}{dt}\begin{bmatrix} x_{POD1} \\ x_{POD2} \\ x_{POD3} \end{bmatrix} = \begin{bmatrix} -\dfrac{\omega_n T_\omega/Q + 1}{T_\omega} & -\dfrac{\omega_n/Q + \omega_n^2 T_\omega}{T_\omega} & -\dfrac{\omega_n^2}{T_\omega} \\ 1 & 0 & 0 \\ 0 & 1 & 0 \end{bmatrix}$$

$$\begin{bmatrix} x_{POD1} \\ x_{POD2} \\ x_{POD3} \end{bmatrix} + \begin{bmatrix} 1 \\ 0 \\ 0 \end{bmatrix} f_{error}^{td} \tag{7}$$

$$P_{POD} = \begin{bmatrix} \omega_n/Q & 0 & 0 \end{bmatrix} \begin{bmatrix} x_{POD1} \\ x_{POD2} \\ x_{POD3} \end{bmatrix} \tag{8}$$

Combining with the outer loop control, inner loop control, and PLL function of the VSC, the small signal model of the complete test system can be obtained after linearization, as shown in (**Eq. 9**).

$$\frac{d\Delta x}{dt} = A\Delta x + B\Delta u \tag{9}$$

where A is a 21×21 state matrix; B is a 21×2 input matrix.

$$A_{SG} = \begin{bmatrix} -\dfrac{E'_{1d0}}{\omega_0 T_{J1}} & -\dfrac{E'_{1q0}}{\omega_0 T_{J1}} & 0 & 0 \\ 0 & 0 & -\dfrac{E'_{2d0}}{\omega_0 T_{J2}} & -\dfrac{E'_{2q0}}{\omega_0 T_{J2}} \end{bmatrix} A_{delay}$$

$$= \begin{bmatrix} -\dfrac{20}{T_d} & -\dfrac{180}{T_d^2} & -\dfrac{840}{T_d^3} & -\dfrac{1680}{T_d^4} \\ 1 & 0 & 0 & 0 \\ 0 & 1 & 0 & 0 \\ 0 & 0 & 1 & 0 \end{bmatrix}$$

$$A_{x\omega} = \begin{bmatrix} 1/2\pi & -1/2\pi \\ 0 & 0 \\ 0 & 0 \end{bmatrix},$$

$$A_{xz} = \begin{bmatrix} -40/T_d & 0 & -1680/T_d^3 & 0 \\ 0 & 0 & 0 & 0 \\ 0 & 0 & 0 & 0 \end{bmatrix},$$

$$A_\omega = \begin{bmatrix} -D_1/T_{J1} & 0 \\ 0 & -D_2/T_{J2} \end{bmatrix}, A_{ii} = \begin{bmatrix} 0 & \omega_0 \\ -\omega_0 & 0 \end{bmatrix}$$

$$a = \begin{bmatrix} 0 & -1/X_f \\ 1/X_f & 0 \end{bmatrix}, b = \frac{3}{2} \cdot \begin{bmatrix} i_{sd0} & i_{sq0} \\ i_{sq0} & -i_{sd0} \end{bmatrix},$$

$$c = \frac{3}{2} \cdot \begin{bmatrix} u_{sd0} & u_{sq0} \\ -u_{sq0} & u_{sd0} \end{bmatrix}, d = \begin{bmatrix} -1/L_1 & 0 \\ 0 & -1/L_1 \end{bmatrix},$$

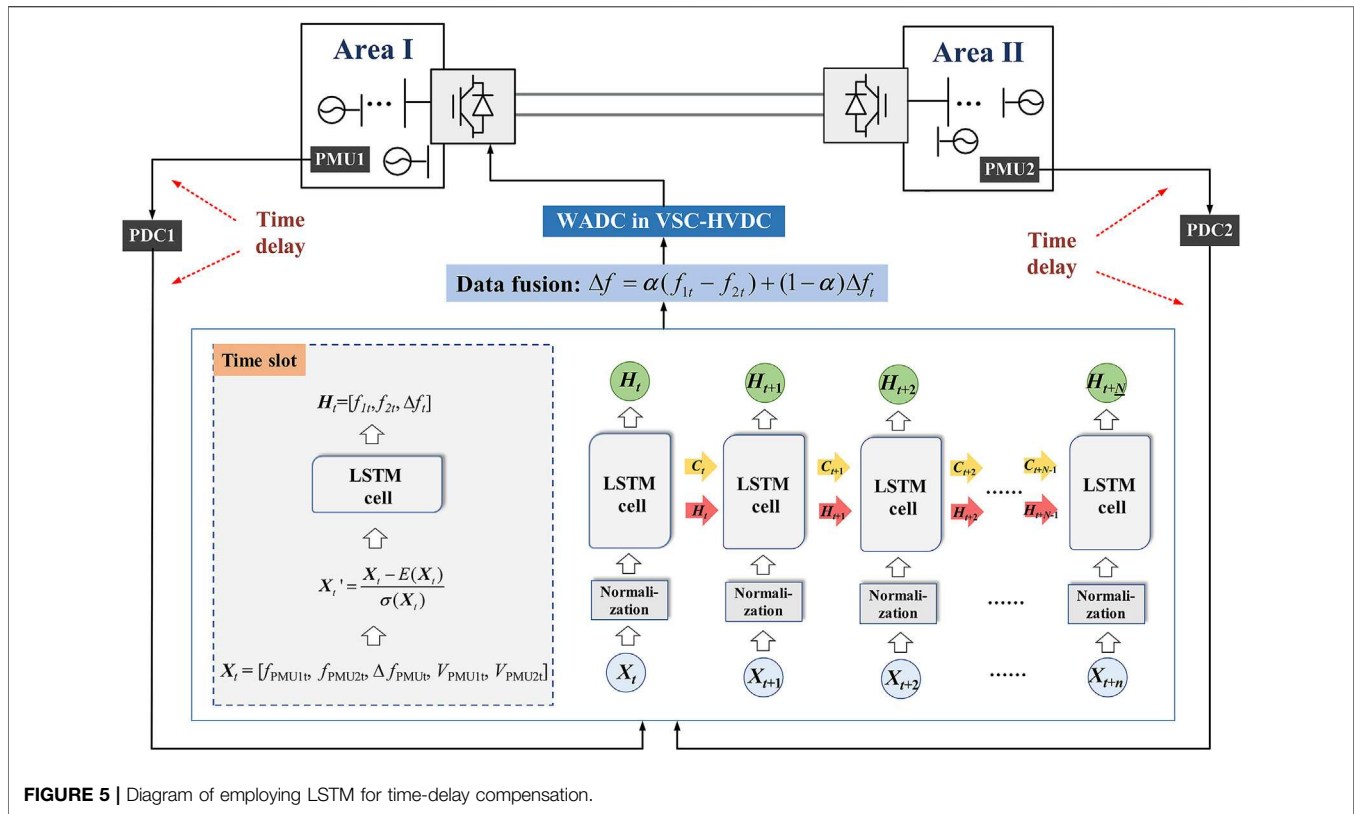$$e = \begin{bmatrix} -1/L_2 & 0 \\ 0 & -1/L_2 \end{bmatrix}$$

FIGURE 5 | Diagram of employing LSTM for time-delay compensation.

$$K_1 = \begin{bmatrix} -\dfrac{\omega_n T_\omega / Q + 1}{T_\omega} & -\dfrac{\omega_n / Q + \omega_n^2 T_\omega}{T_\omega} & -\dfrac{\omega_n^2}{T_\omega} \\ 1 & 0 & 0 \\ 0 & 1 & 0 \end{bmatrix},$$

$$K_{21} = \begin{bmatrix} k_{pp} & 0 \\ 0 & k_{pq} \end{bmatrix}, K_{22} = \begin{bmatrix} k_{ip} & 0 \\ 0 & k_{iq} \end{bmatrix}, K_{31} = \begin{bmatrix} k_{pid} & 0 \\ 0 & k_{piq} \end{bmatrix},$$

$$K_{32} = \begin{bmatrix} k_{iid} & 0 \\ 0 & k_{iiq} \end{bmatrix}, K_4 = \begin{bmatrix} 0 & k_{iPLL} \\ 0 & k_{pPLL} \end{bmatrix}$$

$$M_1 = \begin{bmatrix} \dfrac{3u_{cqo} - 3i_{sd0}X_f}{2X_f} & \dfrac{2u_{s0} - 3u_{cdo} - 3i_{sq0}X_f}{2X_f} \\ \dfrac{-2u_{s0} + 3u_{cdo} - 3i_{sq0}X_f}{2X_f} & \dfrac{3u_{cqo} + 3i_{sd0}X_f}{2X_f} \end{bmatrix},$$

$$M_2 = \begin{bmatrix} \dfrac{3u_{cqo}}{2X_f} & \dfrac{2u_{c0} - 3u_{cdo}}{2X_f} \\ \dfrac{2u_{c0} + 3u_{cdo} - 4u_{s0}}{2X_f} & \dfrac{3u_{cqo}}{2X_f} \end{bmatrix}$$

$$M_3 = I - M_1^{-1}M_2,$$

$$M = (I + a^2 - K_{31}K_{21}K_1 ca + K_{31}a)M_3 - K_{31}K_{21}K_1 b$$

$$A_{PQ} = \begin{bmatrix} -K_{22}K_1(b + caM_3)M^{-1}K_{31} \\ -K_{22}K_1(b + caM_3)M^{-1} \\ K_{22}K_1(b + caM_3)M^{-1}K_{31}K_{21}K_1 \end{bmatrix}^T$$

$$A_{is} = \begin{bmatrix} K_{22} - K_{22}K_{21}K_1(b + caM_3)M^{-1}K_{31} - K_{32}aM_3M^{-1}K_{31} \\ -K_{22}K_{21}K_1(b + caM_3)M^{-1} - K_{32}aM_3M^{-1} \\ K_{22}K_{21} - K_{22}K_{21}K_1(b + caM_3)M^{-1}K_{31}K_{21} - K_{32}aM_3M^{-1}K_{31}K_{21} \end{bmatrix}^T$$

$$A_{ig} = \begin{bmatrix} dM^{-1}K_{31} & eM^{-1}K_{31} \\ dM^{-1} & eM^{-1} \\ -dM^{-1}K_{31}K_{21}K_1 & -eM^{-1}K_{31}K_{21}K_1 \end{bmatrix}^T,$$
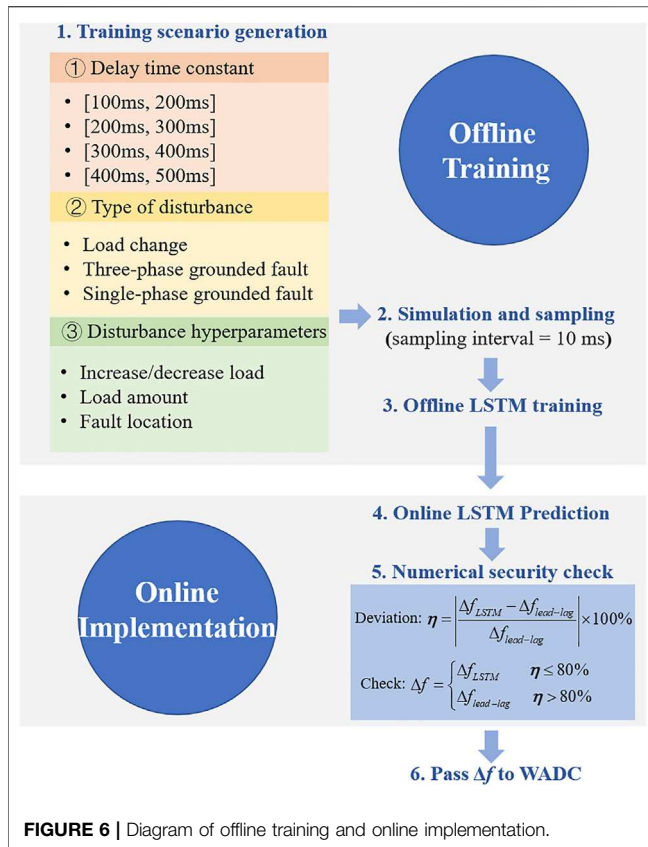
$$A_{PLL} = \begin{bmatrix} K_4 M^{-1}K_{31} \\ K_4 M^{-1} \\ K_4 M^{-1}K_{31}K_{21}K_1 \end{bmatrix}^T$$

Time Delay Analysis

With the established small signal state space model, eigenvalue analysis can be conducted to investigate the stability of the system. As shown in **Figure 3**, the dominant eigenvalue of A is presented with time delay T_d varying from 200 to 500 ms. The other parameters of the test system remain constant.

In **Figure 3**, with the increase of T_d, the dominant eigenvalue gradually moves towards the positive direction of the real-axis. When T_d is greater than 464 ms, the eigenvalue will pass through the imaginary-axis and reach the right half plane of the coordinate axis, indicating that the system becomes unstable.

It can be concluded that: the stability margin of the system is reduced with the increase of the time delay, and even instability

FIGURE 6 | Diagram of offline training and online implementation.

may occur. Therefore, in a VSC-HVDC system with WADC strategy, the time delay issue needs to be carefully resolved to guarantee the system stability.

DATA-DRIVEN DELAY COMPENSATION WITH LSTM

This section firstly gives an overview of LSTM and then employs it on time-delay compensation for WADC.

Preliminaries on LSTM

To improve the numerical instability of RNNs, several tricks such as new structure design are developed and implemented in the sophisticated sequence models. LSTM is one of the promising models that solves the problem of preserving the long-term information and skipping short-term input. **Figure 4** shows the basic cell of LSTM. Apart from the typical input and output, the cell also includes a few gates recurrent units (GRUs), memory, candidate memory, and hidden state. They are illustrated as follows (Zhang A. et al., 2022).

Gate Recurrent Units

There are three gate recurrent units utilized in LSTM: 1). input gate I_t is to decide whether to read data into the cell; 2). output gate O_t is responsible for reading out the entries from the cell; and 3). forget gate F_t is designed for resetting the content of the cell.

The hidden states and the input data are fed to the three units and processed by fully-connected layers with sigmoid activation functions. The output of the three GRUs is calculated as follows.

$$\begin{cases} I_{t+1} = \sigma\left(X_{t+1}W_{xi} + H_tW_{ni} + \mathbf{b}_i\right) \\ F_{t+1} = \sigma\left(X_{t+1}W_{xf} + H_tW_{nf} + \mathbf{b}_f\right) \\ O_{t+1} = \sigma\left(X_{t+1}W_{xo} + H_tW_{no} + \mathbf{b}_o\right) \end{cases} \quad (10)$$

where W_{xi}, W_{xf}, W_{xo}, W_{ni}, W_{nf}, and W_{no} are weight parameters, and $\mathbf{b}_i$, $\mathbf{b}_f$, and $\mathbf{b}_i$ are bias parameters.

Memory and Candidate Memory

LSTM can choose to remember or forget the information from the last time slot, leveraging the input gate and forget gate. First, candidate memory is generated using a tanh function as activation function.

$$\tilde{C}_{t+1} = \tanh\left(X_{t+1}W_{xc} + H_tW_{nc} + \mathbf{b}_c\right) \quad (11)$$

where $\tilde{C}_{t+1}$ is the output of candidate memory. Then, the current cell memory is generated through fusing the past cell memory and candidate memory as follows.

$$C_{t+1} = F_{t+1} \odot C_t + I_{t+1} \odot \tilde{C}_{t+1} \quad (12)$$

where $\odot$ is the Hadamard (elementwise) robust operator. The combination of past cell memory and candidate memory enables the pass of cell memory and thus alleviates the vanishing gradient problem.

Hidden State

As shown in (**Eq. 13**), hidden state H_t is calculated by integrating the current memory into the last hidden state. H_t belongs to [-1, 1] because it is processed by tanh before passed to the next cell.

$$H_t = O_t \odot \tanh\left(C_t\right) \quad (13)$$

With the special designs above, LSTM can finally capture the dependencies from historical data and predict the future value accurately.

Delay Compensation With LSTM

This subsection dives into the implementation of LSTM for delay compensation of WADC.

Fundamental Idea

Figure 5 shows the fundamental idea of the time delay compensation. PMU1 and PMU2 are implemented locally in two urban power grids to measure voltage and frequency. The delay usually happens on the signal transmission from PMU to damping control center. Typically, the delay is within the range of [10 ms, 500 ms], and the delay time constant varies depending on the distance of PUM to damping control center and the types of disturbances. An LSTM is employed locally in the damping control center to correct the sampled data before passing the delayed signals to controllers. In this way, the damping controller can function effectively without worrying about the negative impacts of communication time delay.
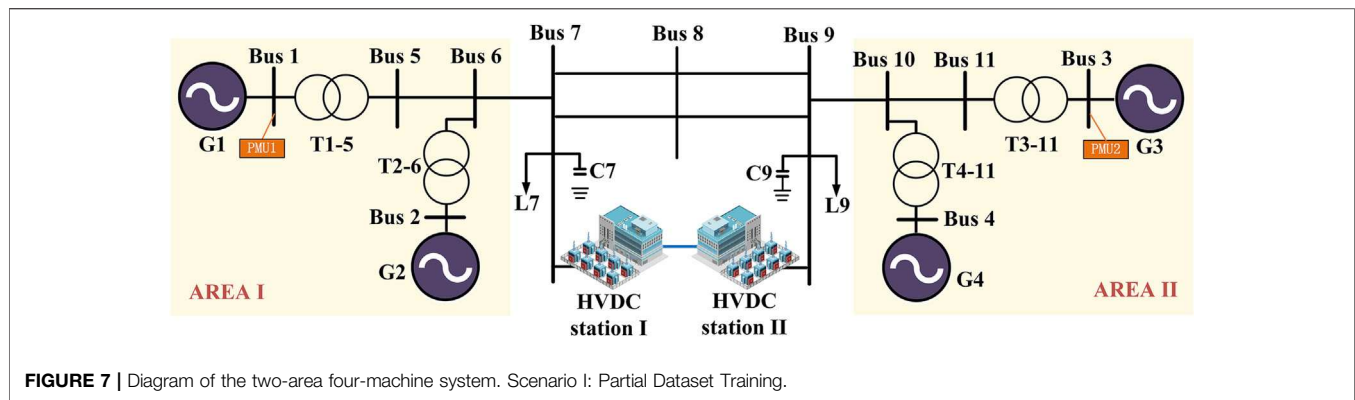
FIGURE 7 | Diagram of the two-area four-machine system. Scenario I: Partial Dataset Training.

TABLE 1 | Training hyperparameter of LSTM.

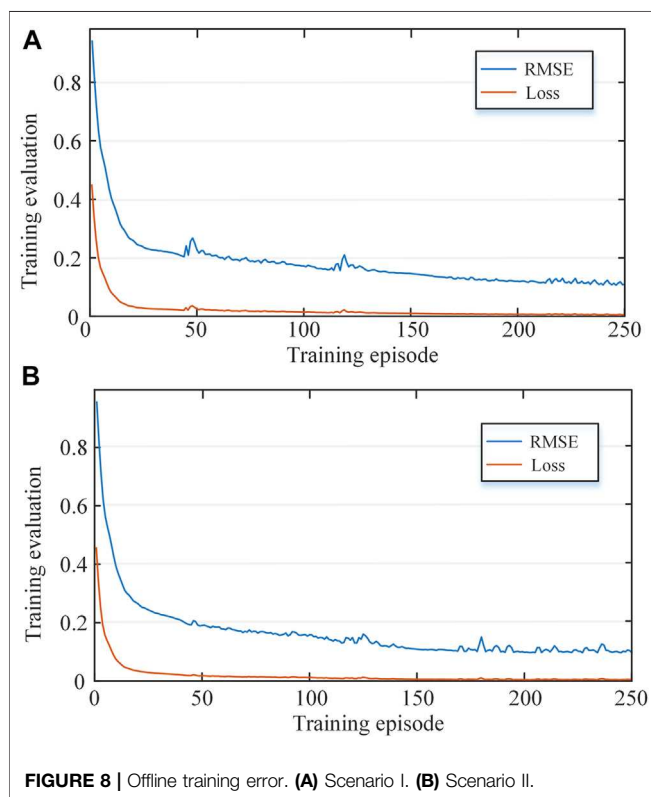| Name	Value
Optimizer	Adam
Initial learning rate	0.005
Learning rate decaying factor	0.2
Learning rate decaying period	125
Maximum episode	250

FIGURE 8 | Offline training error. **(A)** Scenario I. **(B)** Scenario II.

Input-Output Design

LSTM predicts the real time frequency of Area I and Area II based on the delayed data from PMU1 and PMU2. For each time slot, the input data $X_t = [f_{PMU1t}, f_{PMU2t}, \Delta f_{PMUt}, V_{PMU1t},$ $V_{PMU2t}]$. The number of hidden units is denoted by N, representing how far LSTM looks back when correcting the time delay. Then, the input data are normalized before being fed into the LSTM cell. Finally, LSTM outputs the real time f_{1t}, f_{2t}, and Δf_t.

Before feeding the predicted frequency error to damping controller, data fusion is utilized to increase the robustness of the time delay compensation. The final frequency error is calculated by integrating the predicted frequency into the predicted error as follows.

$$\Delta f = \alpha\left(f_{1t} - f_{2t}\right) + (1 - \alpha)\Delta f_t \qquad (14)$$

where α is a hyperparameter that controls the fusion rate. The data fusion can smooth the prediction error and increase the stability of the data-driven approach.

Offline Training and Online Implementation

The strategy of offline training and online implementation is used in this paper. As shown in **Figure 6**, the offline training is three-fold: training scenario generation, simulation and data sampling, and LSTM training, while online implementation includes LSTM prediction, numerical security check, and data passing. They are illustrated in detail in the following subsections.

Offline Training

The training data is generated under various disturbances. With the random combination of the three key elements that determine a disturbance, i.e., delay time constant, type of disturbance, and disturbance hyperparameters, the training data set can cover common disturbances in urban power systems. For each generated disturbance, perform numerical simulation in MATLAB-Simulink and sample the input data with time delay and the output data without time delay. The time interval of sampling is set as 10 ms, which is identical to the PMU sampling rate in reality. Then, all the training data are packaged for LSTM training.

Online Implementation

After extensive training, the well-trained LSTM is ready for online implantation. As shown in **Figure 5**, LSTM network

TABLE 2 | Validation condition.

Scenario	No.	Type of Disturbance	Delay Time Constant (ms)	Disturbance Hyper Parameters	Settings that Are Different from the Training Dataset
Scenario I	1	Load increase	250	Area I, Δp = 300 MW	②③
	2	Load decrease	250	Area II, Δp = -300 MW	②③
	3	Three-phase grounded fault	250	Area I, t = 0.1s (clearing time)	①②③
	4	Single-phase grounded fault	250	Area II, t = 0.1s	①②③
Scenario II	1	Load increase	250	Area I, Δp = 300 MW	②
	2	Load decrease	250	Area II, Δp = -300 MW	②
	3	Three-phase grounded fault	250	Area I, t = 0.1s	②
	4	Single-phase grounded fault	250	Area II, t = 0.1s	②

Note: ① is type of disturbance; ② is delay time constant; ③ is disturbance hyperparameter.

predicts the real time frequency error between the two urban power systems based on the delayed PMU data. To guarantee the security of implementing unexplainable neural network, a numerical security check is performed before passing the predictions to damping controller. The online prediction of LSTM is compared with that of the model-based lead-lag time delay compensator. If the prediction of LSTM deviates less than 80% from the lead-lag controller, the prediction is passed to damping controller. Otherwise, the conventional predictor will be used. The security check is designed to prevent the numerical instability of neural network prediction. Due to the non-interpretability of LSTM, we cannot guarantee that LSTM always predicts the error within an acceptable range. Hence, the model-based lead-lag module is used to generate the interpretable correction signals that are certainly secure. **Eqs 15, 16** show the security check process, which enhances the stability and reliability of the data-driven compensation.

$$\eta = \left| \frac{\Delta f_{LSTM} - \Delta f_{lead-lag}}{\Delta f_{lead-lag}} \right| \times 100\% \qquad (15)$$

$$\Delta f = \begin{cases} \Delta f_{LSTM} & \eta \leq 80\% \\ \Delta f_{lead-lag} & \eta > 80\% \end{cases} \qquad (16)$$

CASE STUDY

This section validates the proposed time-delay compensation approach in a two-area four-machine system.

Case Overview

As shown in **Figure 7**, both Area I and Area II have two synchronous generators supplying local loads, and they are connected through AC transmission lines and VSC-HVDC. The AC transition is responsible for the transmission of active power, while the VSC-HVDC performs wide area damping control based on PMU measurements. PMU1 and PMU2 are equipped at the terminal of G1 and G3, respectively.

To better validate the generalization of the data-driven method, the offline training data is divided into several groups based on delay time constant, type of disturbance, and

disturbance hyperparameters. In Scenario I, LSTM is trained on a dataset of partial disturbances, while in Scenario II, LSTM is trained on a dataset of all kinds of disturbances.

In Scenario I, the training dataset is generated on the disturbance of load change with delay time constant belonging to (100 ms, 200 ms) and (300 ms, 400 ms). Then, conduct LSTM training using the hyperparameters listed in **Table 1**, and the training results are presented in **Figure 8**. After 250 episodes, the LSTM's prediction root mean square error (RMSE) and training loss are both near zero, indicating that the LSTM has a high forecast accuracy on the training dataset.

Assume the fusion rate α = 0.5, the well-trained LSTM is implemented online and tested under the conditions in **Table 2**. The validation results are plotted in **Figure 9A**, based on which we have the following observations.

- Time delay degrades the performance of the WADC. The oscillation becomes severe when directly utilizing the delayed signal from PMU.
- In No.1 and No. 2 validation conditions, although the delay time constant 250 ms doesn't belong to the training dataset, LSTM can still correct the delayed frequency accurately.
- There is a minor oscillation around 4 Hz in No.1 validation condition. The oscillation is outside WADC's target suppression mode, so it is not suppressed considerably.
- In No. 3 and No. 4 validation conditions, LSTM doesn't compensate for the delayed signals well because neither of the three key elements that determine a disturbance belongs to the training dataset. However, the performance of WADC is somewhat improved with the compensation of LSTM.

Scenario II: Complete Dataset Training

To validate the overall performance of LSTM, the dataset of three kinds of disturbance is used for offline training in Scenario II. The delay time constant and the disturbance hyperparameters are identical to those in Scenario II. Using the training hyperparameters in **Table 1**, the LSTM's prediction RMSE and training loss converge to 0 after training for 250 episodes. **Figure 9B** shows the training error, which suggests that LSTM can predict the un-delayed signals accurately.

Assume the fusion rate α = 0.5, the well-trained LSTM is implemented online and tested under the conditions in **Table 2**.

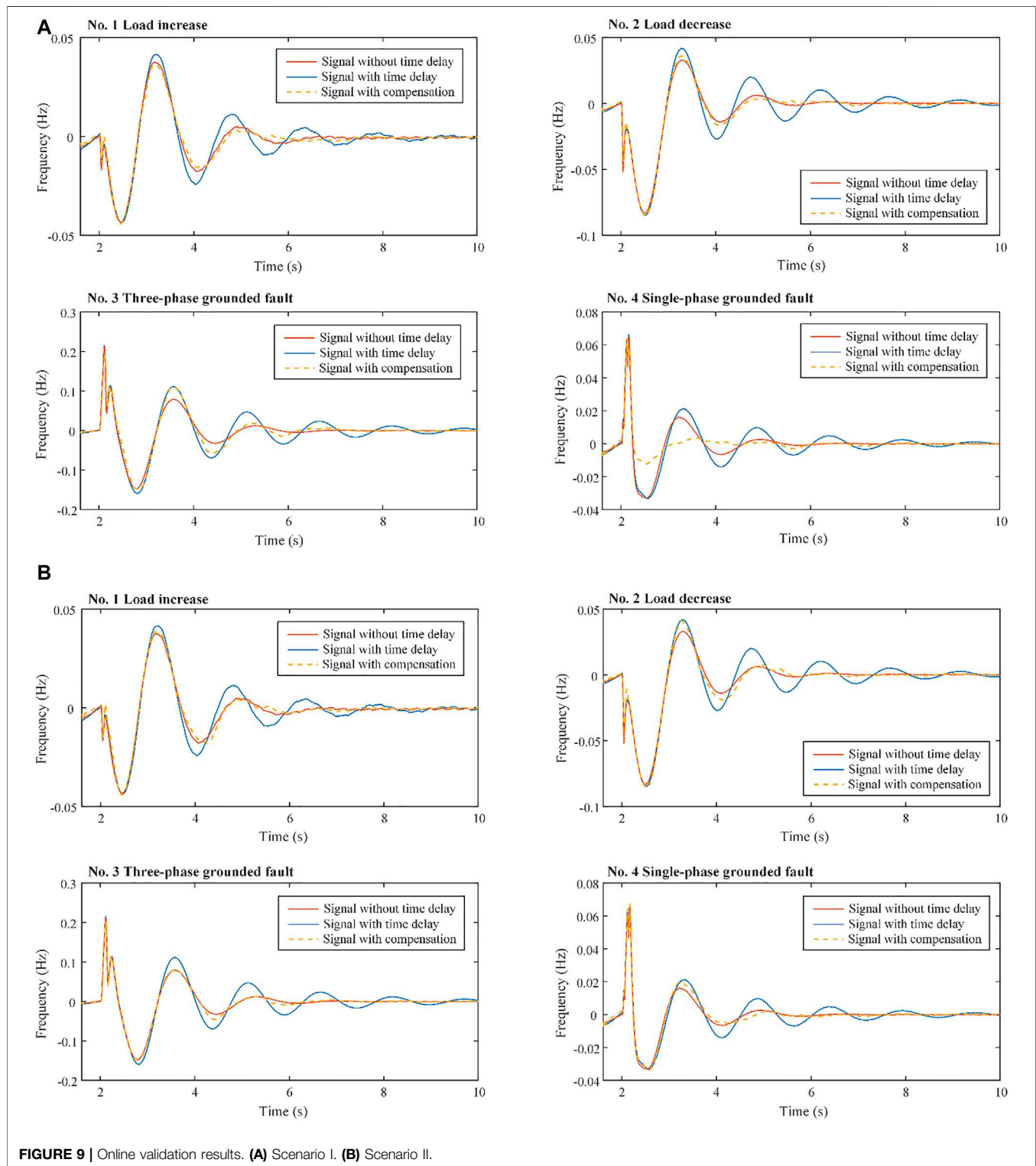FIGURE 9 | Online validation results. (A) Scenario I. (B) Scenario II.

Figure 9 shows the dynamic frequency with and without the compensation. We can see that in the four validation conditions, although the test delay time constant 250 ms doesn't belong to the training dataset, LSTM can predict the error of delay accurately. The performance of WADC's has improved significantly. **Figure 10** further plots the normalized online prediction error, which can be expressed in (**Eq. 17**).
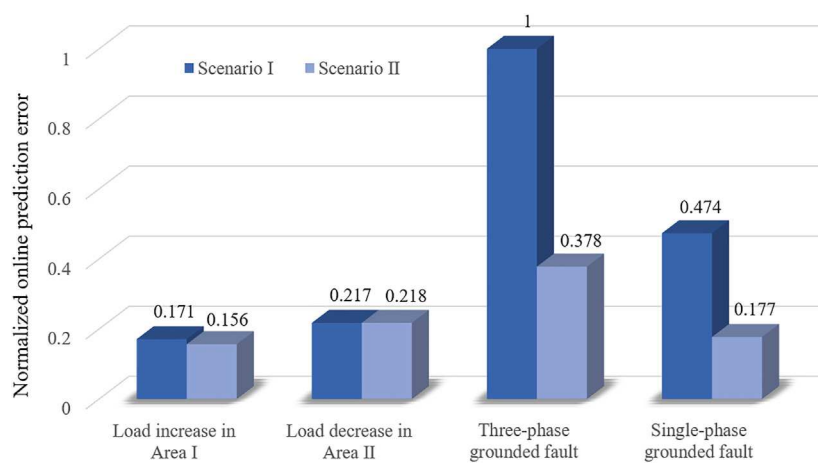
FIGURE 10 | Normalized online prediction error of LSTM in Scenario I and Scenario II.

$$\mathbf{NOPE}_i = \sum_{time} \Delta f_{LSTMi} \Big/ \max\left(\sum_{time} \Delta f_{LSTMi} \right) \qquad (17)$$

where NOPE is the "normalized online prediction error"; i represents the respective case in each scenario.

The NOPE of three-phase grounded fault and single-phase grounded fault in Scenario I is much less than that in Scenario II, indicating that LSTM has insufficient generalization ability for the type of disturbance. Hence, the training dataset should cover all types of disturbance as much as possible in practical application.

In general, a well-trained LSTM can provide accurate correction signals for WADC. It has strong generalization ability for delay time constant, which is beneficial to its employment in real systems. With the delay compensator, WADC can address the random time delay and improve its damping performance significantly.

CONCLUSION

The time delay in WADC can degrade the performance of damping controllers and even results in instability. The root cause is revealed through small signal modeling and eigenvalue analysis in this paper. To address this issue, this paper further proposed a data-driven approach to compensate for the delayed PMU signals, which leverages the modern recurrent neural network LSTM. The compensation procedure includes offline training and online implantation. Through partial dataset training and complete dataset training in a two-area four-machine system, it is verified that LSTM corrects the delayed frequency accurately. LSTM has strong generalization ability for delay time constant and can deal with the random time delay caused by commination and disturbances in urban power grids. After employing the delay correction approach, the damping performance of WADC is improved significantly.

One potential weakness of our work is that LSTM needs as many training data that cover all kinds of disturbances as possible. Our future work may include developing a more efficient training method with less training data, improving the generalization ability of LSTM to handle new disturbances, integrating the topology change into data generation, and validating the data-driven approach in a hardware-in-the-loop system.

DATA AVAILABILITY STATEMENT

The original contributions presented in the study are included in the article/Supplementary Material, further inquiries can be directed to the corresponding author.

AUTHOR CONTRIBUTIONS

BS contributed to conception and design of the study. YD generated the database and implemented simulation. YL provided guidance to the study. BS and YD wrote the draft of the manuscript. All authors contributed to manuscript revision, read, and approved the submitted version.

REFERENCES

Abdelsalam, A. A., Salem, A. A., Oda, E. S., and Eldesouky, A. A. (2020). Islanding Detection of Microgrid Incorporating Inverter Based DGs Using Long Short-Term Memory Network. *IEEE Access* 8, 106471–106486. doi:10.1109/ACCESS.2020.3000872

Alavi, S. A., Mehran, K., Vahidinasab, V., and Catalao, J. P. S. (2021). Forecast-Based Consensus Control for DC Microgrids Using Distributed Long Short-Term Memory Deep Learning Models. *IEEE Trans. Smart Grid* 12, 3718–3730. doi:10.1109/TSG.2021.3070959

Baltas, G. N., Lai, N. B., Tarraso, A., Marin, L., Blaabjerg, F., and Rodriguez, P. (2021). AI-based Damping of Electromechanical Oscillations by Using Grid-Connected Converter. *Front. Energ. Res.* 9, 598436. doi:10.3389/fenrg.2021.598436

Chang, Y., Chen, H., Cheng, G. H., and Xie, J. (2006). "Design of HVDC Supplementary Controller Accommodating Time Delay of the WAMS Signal in Multi-Machine System," in *IEEE Power Engineering Society General Meeting*. Montreal, QC, Canada: IEEE, 7. doi:10.1109/PES.2006.1709071

Chaudhuri, B., Majumder, R., and Pal, B. C. (2004). Wide-area Measurement-Based Stabilizing Control of Power System Considering Signal Transmission Delay. *IEEE Trans. Power Syst.* 19, 1971–1979. doi:10.1109/TPWRS.2004.835669

Cheng, L., Chen, G., Gao, W., Zhang, F., and Li, G. (2014). Adaptive Time Delay Compensator (ATDC) Design for Wide-Area Power System Stabilizer. *IEEE Trans. Smart Grid* 5, 2957–2966. doi:10.1109/TSG.2014.2347401

Dong, Y., Ma, J., Wang, S., Liu, T., Chen, X., and Huang, H. (2021). An Accurate Small Signal Dynamic Model for LCC-HVDC. *IEEE Trans. Appl. Supercond.* 31, 1–6. doi:10.1109/TASC.2021.3107804

Fu, Y., Hu, C.-H., and Yang, D.-X. (2021). Conservative or Aggressive? the Dynamic Adjustment of the Feed-In Tariff Policy for Photovoltaic Power Generation in China. *Front. Energ. Res.* 9, 672920. doi:10.3389/fenrg.2021.672920

He, J., Wu, X., Li, P., Lu, C., and Wu, J. (2009). Design and experiment of Wide Area HVDC Supplementary Damping Controller Considering Time Delay in China Southern Power Grid. *IET Generation, Transm. Distribution* 3, 17–25. doi:10.1049/iet-gtd:20080129

Jiang, X., Xiao, J., She, B., and Zu, G. (2019). Locating and Sizing of Partition Flexible Interconnection Converter Station in Large Urban Power Grids. *IET Generation, Transm. & Distribution* 13, 4830–4841. doi:10.1049/iet-gtd.2018.6871

Li, M., and Chen, Y. (2018). A Wide-Area Dynamic Damping Controller Based on Robust H∞ Control for Wide-Area Power Systems with Random Delay and Packet Dropout. *IEEE Trans. Power Syst.* 33, 4026–4037. doi:10.1109/TPWRS.2017.2782792

Li, S., Hou, J., Yang, A., and Li, J. (2021). DNN-based Distributed Voltage Stability Online Monitoring Method for Large-Scale Power Grids. *Front. Energ. Res.* 9. doi:10.3389/fenrg.2021.625914

Li, Y., Rehtanz, C., Yang, D. C., Gorner, K., Ruberg, S., and Luo, L. F. (2010). "Wide-area Time-Delay Damping Control to Prevent Power Oscillations in HVDC/AC Interconnected Power Systems," in 2010 International Conference on Power System Technology. Zhejiang, China: IEEE, 1–6. doi:10.1109/POWERCON.2010.5666549

Li, Z., Liu, H., Zhao, J., Bi, T., and Yang, Q. (2021). Fast Power System Event Identification Using Enhanced LSTM Network with Renewable Energy Integration. *IEEE Trans. Power Syst.* 36, 4492–4502. doi:10.1109/TPWRS.2021.3064250

Liu, B., Chen, J., Wang, H., and Wang, Q. (2020). Renewable Energy and Material Supply Risks: a Predictive Analysis Based on an LSTM Model. *Front. Energ. Res.* 8, 163. doi:10.3389/fenrg.2020.00163

Musleh, A. S., Muyeen, S. M., Al-Durra, A., Kamwa, I., Masoum, M. A. S., and Islam, S. (2018). Time-Delay Analysis of Wide-Area Voltage Control Considering Smart Grid Contingences in a Real-Time Environment. *IEEE Trans. Ind. Inf.* 14, 1242–1252. doi:10.1109/TII.2018.2799594

Pan, G., Hu, Q., Gu, W., Ding, S., Qiu, H., and Lu, Y. (2021). Assessment of Plum Rain's Impact on Power System Emissions in Yangtze-Huaihe River basin of China. *Nat. Commun.* 12, 6156. doi:10.1038/s41467-021-26358-w

Sun, K., Li, K.-J., Zhang, Z., Liang, Y., Liu, Z., and Lee, W.-J. (2022). An Integration Scheme of Renewable Energies, Hydrogen Plant, and Logistics Center in the Suburban Power Grid. *IEEE Trans. Ind. Applicat.* 58, 2771–2779. doi:10.1109/TIA.2021.3111842

Sun, K., Qiu, W., Yao, W., You, S., Yin, H., and Liu, Y. (2021a). Frequency Injection Based HVDC Attack-Defense Control via Squeeze-Excitation Double CNN. *IEEE Trans. Power Syst.* 36, 5305–5316. doi:10.1109/TPWRS.2021.3078770

Sun, K., Xiao, H., Pan, J., and Liu, Y. (2021b). VSC-HVDC Interties for Urban Power Grid Enhancement. *IEEE Trans. Power Syst.* 36, 4745–4753. doi:10.1109/TPWRS.2021.3067199

Wang, M., Liu, J., and Liu, J. (2010). "Delay-dependent Robust H∞ Control of Nonlinear Uncertain Time-Delay Systems," in *IEEE ICCA*. Xiamen, China: IEEE, 1249–1254. doi:10.1109/ICCA.2010.5524229

Wang, Q., Bu, S., He, Z., and Dong, Z. Y. (2021). Toward the Prediction Level of Situation Awareness for Electric Power Systems Using CNN-LSTM Network. *IEEE Trans. Ind. Inf.* 17, 6951–6961. doi:10.1109/TII.2020.3047607

Xiao, H., Sun, K., Pan, J., Li, Y., and Liu, Y. (2021). Review of Hybrid HVDC Systems Combining Line Communicated Converter and Voltage Source Converter. *Int. J. Electr. Power Energ. Syst.* 129, 106713. doi:10.1016/j.ijepes.2020.106713

Xiao, J., Cai, Z., Liang, Z., and She, B. (2022). Mathematical Model and Mechanism of TSC Curve for Distribution Networks. *Int. J. Electr. Power Energ. Syst.* 137, 107812. doi:10.1016/j.ijepes.2021.107812

Xiong, M., Xu, X., Sun, K., and Wang, B. (2021). "Approximation of the Frequency-Amplitude Curve Using the Homotopy Analysis Method," in *2021 IEEE Power Energy Society General Meeting (PESGM)*. Washington, DC, United States: IEEE, 1–5. doi:10.1109/PESGM46819.2021.9638009

Xu, J., Guo, C., Peng, Y., Yang, S., and Zhao, C. (2020). "Small Signal Model of VSC-HVDC Considering the Impact of Time Delay," in 2020 10th International Conference on Power and Energy Systems (ICPES), 286–291. doi:10.1109/ICPES51309.2020.9349709

Xu, Y., Gao, W., Qian, F., and Li, Y. (2021). Potential Analysis of the Attention-Based LSTM Model in Ultra-short-term Forecasting of Building HVAC Energy Consumption. *Front. Energ. Res.* 9. doi:10.3389/fenrg.2021.730640

Yang, D., Jin, Z., Zheng, T., and Jin, E. (2022). An Adaptive Droop Control Strategy with Smooth Rotor Speed Recovery Capability for Type III Wind Turbine Generators. *Int. J. Electr. Power Energ. Syst.* 135, 107532. doi:10.1016/j.ijepes.2021.107532

Zhang, A., Lipton, Z. C., Li, M., and Smola, A. J. (2022). *Dive into Deep Learning*, 1027.

Zhang, J., She, B., Peng, J. C.-H., and Li, F. (2022). A Distributed Consensus-Based Optimal Energy Management Approach in DC Microgrids. *Int. J. Electr. Power Energ. Syst.* 140, 108015. doi:10.1016/j.ijepes.2022.108015

Zhu, L., Liu, H., Pan, Z., Liu, Y., Farantatos, E., Patel, M., et al. (2016). "Adaptive Wide-Area Damping Control Using Measurement-Driven Model Considering Random Time Delay and Data Packet Loss," in *2016 IEEE Power and Energy Society General Meeting (PESGM)*. Boston, MA, United States: IEEE, 1–5. doi:10.1109/PESGM.2016.7741971